Validation of a Freeze-Lining Solidification Model Using Laboratory Experiments Under Static and Dynamic Flow Conditions

Validation of a Freeze-Lining Solidification Model Using Laboratory Experiments Under Static and Dynamic Flow Conditions

Christian M. G. Rodrigues[1], Menghuai Wu[1*], Haijie Zhang[1], Zilong Qiu[2], Annelies Malfliet[2], Muxing Guo[2], Anton Ishmurzin[3], Gernot Hackl[3], Abdellah Kharicha[1]

[1] Metallurgy Department, Montanuniversität Leoben, Leoben, Austria
[2] Department of Materials Engineering, Katholieke Universiteit Leuven, Leuven, Belgium
[3] Department of Modeling and Simulation, RHI Magnesita, Leoben, Austria

[*]E-mail: menghuai.wu@unileoben.ac.at

Abstract. This study attempts to simulate the solidification of slag (non-metallic compounds) in a forced flow condition. The formation of the freeze-lining (FL), i.e. a solidified layer of slag on industry furnace wall, is an important phenomenon in many metallurgical processes. To validate the numerical model, laboratory experiments, involving the immersion of a gas-cooled probe into a molten slag bath, were conducted under controlled conditions for both static and rotating crucibles. A computational fluid dynamics (CFD) model, that coupled a single-phase flow model with a mixture continuum solidification model, was used to simulate these experiments. While the model had been successfully applied to different cases of metal solidification, it was modified for slag solidification. The effect of Euler, centrifugal, and Coriolis forces on the flow was incorporated with the Boussinesq approximation. Data from experiments were used to determine critical material properties and boundary conditions, as well as to validate the model's predictions. The strong agreement between simulations and experiments confirmed the predictive capabilities of the model.

1. Introduction

The solidification and re-melting of slag have traditionally received limited attention within the broader field of solidification. However, freeze-lining (FL) formation, a solidified slag layer, has recently gained significant interest from researchers due to its critical role in protecting refractory linings and its significant impact on overall energy efficiency. As such, FL formation has become a key consideration in the design and operation of numerous pyrometallurgical processes. This FL in industry furnaces enhances thermal insulation, reduces refractory wear, and improves energy efficiency [1].

Laboratory-scale experiments, such as the cooled-probe (finger) experiment, are widely used to study FL formation. A water- or air-cooled probe is immersed in a molten slag bath, allowing a solidified layer (i.e., the FL) to gradually form. This experiment can be performed under both static or dynamic flow conditions. With rotating crucibles, fluid dynamics are influenced by both natural

convection and forced flow (i.e. bath agitation), which significantly impact the FL development and microstructure [2] while providing similar insights as real-world applications.

Existing research has demonstrated that the FL microstructure is strongly affected by cooling rates, slag composition, and thermophysical properties [3-5]. Rapid cooling leads to fine-grained, glassy, or metastable phases with reduced crystallinity [3]. Conversely, slower cooling rates favour the growth of larger, well-defined crystals, which enhance mechanical integrity but increase porosity and susceptibility to slag infiltration [4,5]. Verscheure et al. [3] found that higher slag viscosity, due to components like silica (SiO_2) and alumina (Al_2O_3), stabilized the FL by limiting convective transport at the interface between FL and slag bath. Conversely, lower-viscosity slags enhance fluid motion, leading to FL thinning through erosion and leakage [6]. Experiments by Fallah-Mehrjardi et al. [7,8] further demonstrated the crucial role of mobile crystal dynamics in the FL microstructure and confirmed that the FL thickness is not solely dictated by thermodynamic equilibrium.

A thorough understanding of these interacting factors is essential for optimizing FL performance and longevity in industrial applications, and numerical modelling plays a critical role in achieving this. Early 1D models provided only basic insights [9], but more advanced CFD-based approaches have since emerged [10,11]. Campbell et al. [10] coupled CFD with thermo-mechanics, while Guevara [11] employed the enthalpy-porosity technique; however, neither fully captured the detailed dynamics of FL formation. Recently, we developed a more comprehensive model framework to simulate an electric smelting furnace [12]. The simulation results yielded reasonable predictions of FL thickness, demonstrating its dependence on fluid flow, mass transfer during FL formation, and energy transport. The model framework was later adapted to simulate FL formation in an electrically-powered slag fuming furnace [13]. It incorporated multiphase dynamics and splash-induced FL, and good agreement with industrial data was demonstrated.

The existing model framework could be used to capture FL formation in the laboratory experiment with static crucibles. However, to extend its applicability to rotating crucibles, the inclusion of centrifugal, Coriolis, and Euler forces is necessary. Furthermore, incorporating temperature-dependent density variations in the centrifugal force term, in addition to the gravitational term (within the Boussinesq approximation) was found to be essential for accurately capturing the flow behaviour [14,15].

This research combined experimental investigation with an enhanced CFD model to investigate freeze lining (FL) formation under static and rotating flow conditions. The laboratory experiments provided valuable data for model setup and validation. The validated model serves as a valuable tool for predicting FL behaviour, with potential applications in industrial processes.

2. Experimental and numerical approaches

2.1 Laboratory experiment

The experiment setup consisted of a nitrogen-gas-cooled probe (42 L/min flow rate) immersed in a crucible containing molten slag bath. The crucible, which could be rotated or held stationary, had an 80 mm inner diameter and held a 30 mm deep slag bath. The probe, with an outer diameter of 8 mm, was vertically adjustable, allowing it to be inserted or withdrawn from the slag bath. When immersed, it was positioned 7 mm above the crucible bottom. The probe rotation speed was adjustable between 0 and 10 rpm. Temperature measurements were recorded during the experiment using thermocouples fixed to the probe structure. Additionally, mobile thermocouples were used for supplementary measurements at the end of the experiments.

The experiment comprised three distinct stages (Fig. 1):

- Stage 1.
  Before immersing the probe, the molten slag was left undisturbed for four hours to establish a steady thermal profile. At the end of this period, temperature measurements were taken at two locations: near the sidewall and at the centre of the slag bath (black and grey dots in Fig. 1a, respectively). These measurements were used to define the thermal boundary conditions for the crucible's side and bottom walls in the model.
- Stage 2.
  The probe was immersed in the slag bath for 1, 5, 30, and 60 minutes to induce FL formation. During immersion, the temperature was recorded at two locations: one within the slag bath and another within the developing FL layer (black and grey dots in Fig. 1b, respectively). Additionally, the temperature difference between the inlet and outlet gas from the probe was measured. The slag temperature was used to validate the model, whereas the gas temperature was used to estimate the heat fluxes and define the thermal boundary conditions for the probe's surface in the model.
- Stage 3.
  Immediately after each immersion period, the probe was removed and temperature measurements were taken at three locations (black dots in Fig. 1c). Each sample was then photographed and analysed, and the FL thickness was measured for further model validation. In addition, the as-solidified slag on the probe was also subjected to further metallographic analysis to examine its microstructure.

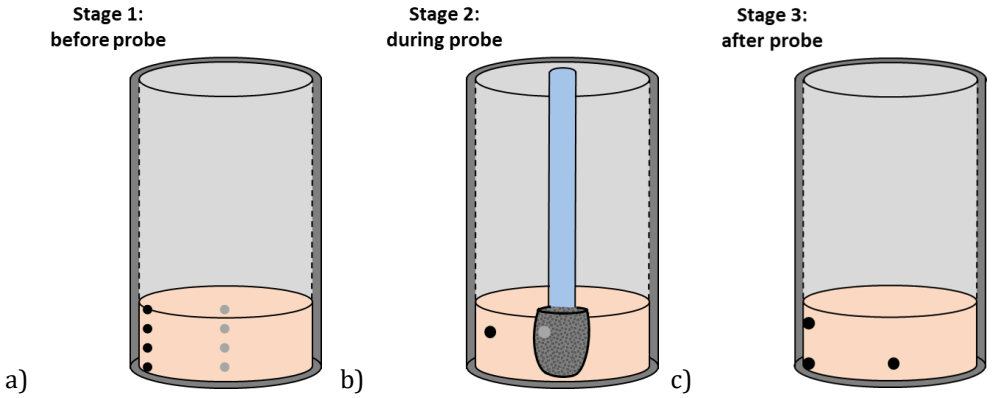

Figure 1. Schematic diagram of the experimental procedure: a) Stage 1 (before probe immersion), b) Stage 2 (during probe immersion), and c) Stage 3 (after probe immersion). Black and grey dots indicate temperature measurement locations at each stage.

2.2 Model settings

Since a detailed description is provided in [12], only a brief outline is given here. The model framework coupled a single-phase flow model with a mixture continuum solidification model. The latter was originally developed for metal alloy solidification [16], but was here adapted to capture slag solidification.

The model solves for mass, momentum and energy conservation equations, as shown in Table 1. To accurately simulate the rotating crucible experiment, the momentum equation was modified to account for rotation and buoyancy effects. Notably, the moving reference frame (MRF) technique was employed with a relative velocity formulation, $\vec{u}_r$. The effects of Euler, centrifugal, and Coriolis forces were included in the momentum equation (where $\vec{\omega}$ is the angular velocity

relative to the inertial reference frame and $\vec{r}$ is the position vector from the origin of the rotating frame). Additionally, the temperature-dependent density variations (ρ') in both gravity and centrifugal force terms were considered within the Boussinesq approximation [14]. To enhance numerical stability, the terms associated with the constant reference density (ρ_{ref}) in the gravity and centrifugal forces were incorporated into a modified pressure, p^*. The final term in the momentum equation represents the drag. In the enthalpy equation, the last term explicitly accounts for the release of latent heat (L) during solidification. This explicit treatment is necessary because an equal heat capacity was assumed for the liquid and solid phases. The solid fraction of slag is denoted by f_s and its thermal conductivity (k_c) is 0.07 W/(m·K).

Table 1. Governing equations for slag solidification problem, with relative velocity formulation and rotational forces.

Equations
$\nabla \cdot \vec{u}_r = 0$
$\rho_{ref} \frac{\partial}{\partial t}(\vec{u}_r) + \rho_{ref} \nabla \cdot (\vec{u}_r \vec{u}_r) = -\nabla p^* + \nabla \cdot \tau + \rho' \vec{g} - \rho_{ref} (\frac{\partial \vec{\omega}}{\partial t} \times \vec{r}) - \rho_{ref} 2\vec{\omega} \times \vec{u}_r - \rho' (\vec{\omega} \times (\vec{\omega} \times \vec{r})) - K_0 \frac{f_s^2}{(1-f_s)^3} \vec{u}_r$
$\rho_{ref} \frac{\partial}{\partial t}(h) + \rho_{ref} \nabla \cdot (\vec{u}_r h) = \nabla \cdot (k_c \nabla T) + \rho_{ref} L \frac{\partial f_s}{\partial t}$

Given that the laboratory experiment involved a slag bath occupying only a small portion of the crucible, the computational domain was simplified to model only the slag region. This simplification assumed a static, horizontal slag-gas interface and neglected potential interfacial deformations during the rotation of the crucible. Two distinct configurations were used for Stage 1 (before probe insertion) and Stage 2 (during probe insertion), as illustrated in Fig. 2a and 2b. The primary difference between these configurations was the inclusion of a volume inside the slag bath in Stage 2 to represent the gas-cooled probe. Note that the experimental procedure also included Stage 3 for post-immersion analysis of FL thickness and temperature. However, this stage was omitted in the model, as these results were directly accessible at the end of Stage 2.

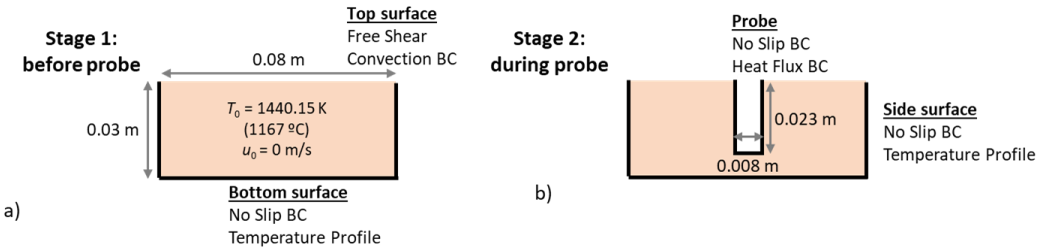

Figure 2. Computational domain with initial and boundary conditions for a) Stage 1 (molten slag before probe immersion), b) Stage 2 (molten slag with immersed probe).

The simulation workflow consisted of three steps: 1) running the simulation for Stage 1; 2) mapping the final flow and temperature fields from Stage 1 as the initial conditions for Stage 2;

3) running the simulation for Stage 2. Simulation results were compared against experimental data at the end of Stage 1, throughout Stage 2, and at the end of Stage 2. The same workflow and computational grids were used for both static and rotating crucible conditions. A detailed description of all the material properties and process parameters used in the simulations is given in Ref. [17].

The computational domain was discretized using a mesh with 0.8 million cells. The model was implemented in ANSYS FLUENT 17.2. A constant time-step size was used, adjusted based on simulation complexity: 0.1 seconds for the static case without the probe (Stage 1, static conditions) and 0.001 seconds for the rotating case with the probe (Stage 2, rotating conditions). These time-step sizes ensured numerical stability and convergence. The simulations were executed on a high-performance computing cluster using 12 CPU cores, with runtimes ranging from one to three weeks, depending on the case.

3. Results

The experiments with static and rotating crucible conditions in Stage 1 produced temperature measurements both near the crucible wall and at the centre (at locations identified in Fig. 1a). To establish appropriate boundary conditions for the model, a parameter study was performed to determine the temperature profile at the crucible walls, and the heat transfer coefficient for the convective boundary conditions at the slag top surface. The parameter study was iterated until a satisfactory agreement was achieved between the simulated and experimental temperature profiles near the wall and at the centre.

Figure 3 shows the comparison between simulation results and experimental data for the temperature profiles near the wall and at the centre, at the end of Stage 1, for both static (Fig. 3a) and rotating (Fig. 3b) crucibles. The best agreement was achieved by using a convective boundary condition on the top surface with a heat transfer coefficient (HTC) of 200 W/m^2/K and a reference temperature (T_{ref}) of 1424 K. The results were highly sensitive to the slag thermal conductivity, for which experimental data was limited. A slag thermal conductivity of 0.07 W/(m·K) provided the best agreement.

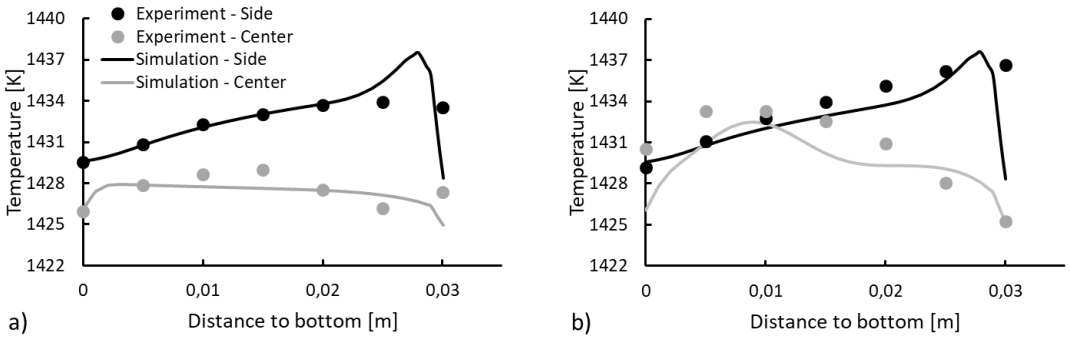

Figure 3. Comparison between simulation results and experimental measurements of temperature near crucible wall and at the centre for a) static, and b) rotating crucible.

The model was validated by comparing simulation results against laboratory experiments for the evolution of the FL thickness, under static (Fig. 4a) and rotating (Fig. 4b) crucibles. The experimental data (black dots) were obtained at 1, 5, 30, and 60 minutes. In both cases, the results demonstrate good agreement between the simulations and experimental data, which further

confirms the model's reliability and reinforces its suitability for studying FL formation under dynamic conditions.

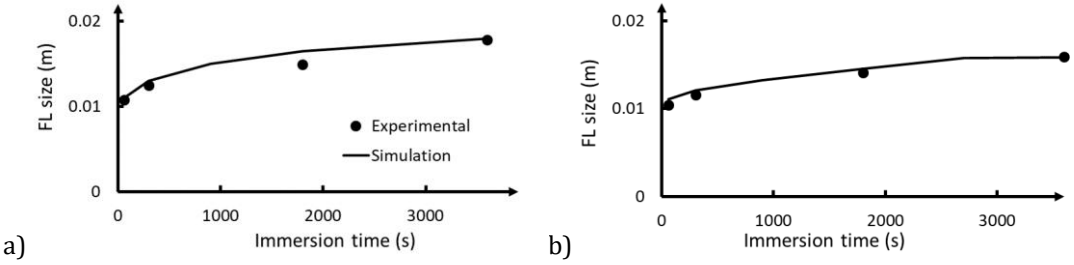

Figure 4. Comparison between simulation results and experimental measurements of FL size evolution for a) static, and b) rotating crucible conditions.

Figure 5 illustrates the simulated evolution of the FL over time, comparing solid fraction, temperature distribution, and velocity fields within the crucible. The left half of each subfigure depicts the solid fraction, ranging from 0 (fully liquid) to 1 (fully solid), indicating the progression of solidification. The right half shows the temperature distribution, bounded between 1415 K (blue) and 1430 K (red) to enhance visualization of the thermal distribution. Superimposed on the temperature distribution are velocity vectors, where arrow size indicates magnitude with an absolute maximum of 0.5 mm/s.

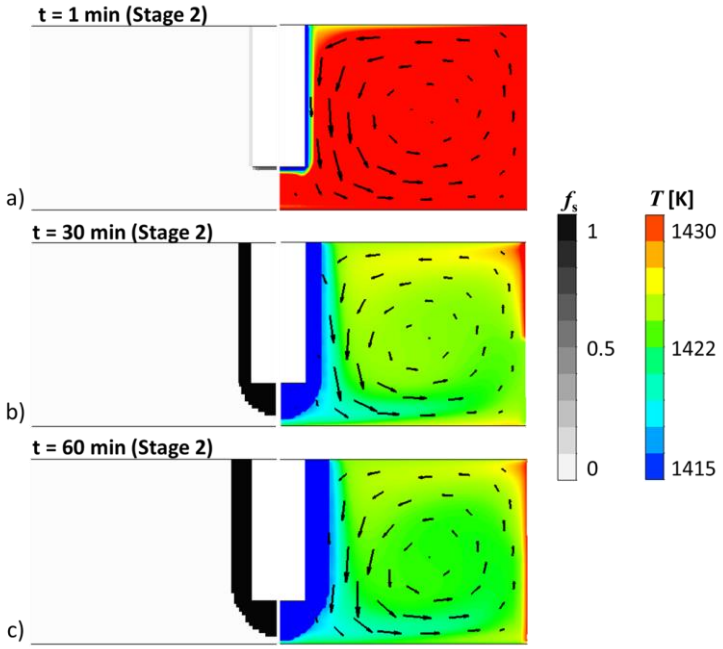

Figure 5. Simulation results at a) 1 min, b) 30 min, and c) 60 min. Left: Solid fraction. Right: Temperature distribution with superimposed velocity vectors (arrow size indicates magnitude, maximum = 0.5 mm/s).

At t = 1 minute (Stage 2, Figure 5a), a minimal FL layer is observed, with the temperature predominantly above 1430 K except in the immediate vicinity of the probe, where the temperature drops below 1415 K (blue cells on right side). Given that the liquidus temperature is

1416.75 K, solidification starts in this region (light grey cells on left side). The velocity field shows a counter-clockwise circulation pattern, driven by thermal gradients. As time progresses (t = 30 minutes, Figure 5b, and t = 60 minutes, Figure 5c), the FL thickness increases noticeably, as evidenced by the expanding solid fraction region. Simultaneously, the temperature distribution evolves, with a cold region developing at the bottom centre and a hot region extending from the top side towards the top centre. This thermal stratification is a direct consequence of the counter-clockwise flow field, which transports heat within the crucible and can influence the shape of the FL layer.

4. Conclusions

This study integrated experimental and numerical methodologies to advance the understanding of FL formation. Laboratory experiments, conducted under both static and rotating crucible conditions, provided crucial data for model development and validation. The model was enhanced to accurately capture the complex fluid dynamics in rotating systems.

Preliminary experiments and numerical parametric studies established reliable simulation conditions. Specifically, a convective boundary condition with an HTC of 200 $W/m^2/K$ and a T_{ref} of 1424 K, along with a slag thermal conductivity of 0.07 W/(m·K), achieved good agreement between simulated and experimental temperature profiles. Validation against FL thickness measurements confirmed the model's reliability for both static and rotating crucible conditions.

This research established a robust framework for predicting and understanding FL behaviour through modelling, which could be applied to process optimization and control in various slag-related industrial pyrometallurgical processes. Despite its effectiveness, the mixture-continuum model oversimplified the FL crystal morphology by treating it as static. Future work will extend the model framework by incorporating a mobile morphology, allowing for a more accurate representation of the FL structure and dynamics. In addition, a more detailed analysis of the current findings and methodologies will be presented in a subsequent publication.

Acknowledgment

This study was supported by the Austrian Research Promotion Agency (FFG) under the framework of the Bridge 1 program (MoSSoFreez Project, grant no. F0999888120 and VERTINGOT project, grant no. FO999903571).

References

[1] Bellemans I, Zietsman J, Verbeken K. Fundamental and Formation Aspects of Slag Freeze Linings: A Review. Journal of Sustainable Metallurgy. 2022;8:64-90. doi:10.1007/s40831-022-00505-z.

[2] Campforts M, Verscheure K, Boydens E, Van Rompaey T, Blanpain B, Wollants P. On the Microstructure of a Freeze Lining of an Industrial Nonferrous Slag. Metallurgical and Materials Transactions B. 2007;38:841-851. doi:10.1007/s11663-007-9099-1.

[3] Verscheure K, Campforts M, Verhaeghe F, Boydens E, van Camp M, Blanpain B, Wollants P. Water-cooled probe technique for the study of freeze lining formation. Metallurgical and Materials Transactions B. 2006;37:929-940. doi:10.1007/BF02735015.

[4] Campforts M, Blanpain B, Wollants P. The importance of slag engineering in freeze-lining applications. Metallurgical and Materials Transactions B. 2009;40:643-655. doi:10.1007/s11663-009-9258-7.

[5] Campforts M, Jak E, Blanpain B, Wollants P. Freeze-lining formation of a synthetic lead slag: Part I. microstructure formation. Metallurgical and Materials Transactions B. 2009;40:619-631. doi:10.1007/s11663-009-9256-9.

[6] Jansson J, Taskinen P, Kaskiala M. Freeze lining formation in continuous converting calcium ferrite slags. I. Canadian Metallurgical Quarterly. 2014;53:1-10. doi:10.1179/1879139513Y.0000000100.
[7] Fallah-Mehrjardi A, Hayes PC, Jak E. Investigation of freeze-linings in copper-containing slag systems: Part II. Mechanism of the deposit stabilization. Metall Mater Trans B. 2013;44:549-560. doi: 10.1007/s11663-013-9807-y.
[8] Fallah-Mehrjardi A, Hayes PC, Jak E. Further experimental investigation of freeze-lining/bath interface at steady-state conditions. Metall Mater Trans B. 2014;45:2040-2049. doi: 10.1007/s11663-014-0149-1.
[9] Wei C, Chen J, Welch B, Voller V. Modelling of dynamic ledge heat transfer. In: Proceedings of the 1997 TMS Annual Meeting; 1997; Orlando, FL, USA.
[10] Campbell AP, Pericleous KA, Cross M. Modelling of freeze layers and refractory wear in direct smelting processes. In: Proceedings: ironmaking conference; 2002; Nashville, Tennessee, USA.
[11] Guevara F. Study of slag freezing in metallurgical furnaces [PhD thesis]. McMaster University, Canada; 2007.
[12] Rodrigues CMG, Wu M, Ishmurzin A, Hackl G, Voller N, Ludwig A, Kharicha A. Modeling framework for the simulation of an electric smelting furnace considering freeze lining formation. Metallurgical and Materials Transactions B. 2023;54:880-894. doi:10.1007/s11663-023-02733-4.
[13] Rodrigues CMG, Wu M, Chintinne M, Ishmurzin A, Hackl G, Lind C, Kharicha A. Modeling freeze-lining formation: a case study in the slag fuming process. Steel Research International. 2024;2400618. doi:10.1002/srin.202400618.
[14] Lopez JM, Marques F. Centrifugal effects in rotating convection: nonlinear dynamics. Journal of Fluid Mechanics. 2009;628:269-297. doi:10.1017/S0022112009006193.
[15] Marques F, Mercader I, Batiste O, Lopez JM. Centrifugal effects in rotating convection: axisymmetric states and three-dimensional instabilities. Journal of Fluid Mechanics. 2007;580:303-318. doi:10.1017/S0022112007005447.
[16] Voller VR, Brent AD, Prakash C. The modelling of heat, mass and solute transport in solidification systems. International Journal of Heat and Mass Transfer. 1989;32:1719-1731. doi:10.1016/0017-9310(89)90054-9.
[17] Rodrigues CMG, Wu M, Qiu Z, Malfliet A, Guo M, Ishmurzin A, Hackl G, Kharicha A. In preparation.